University of Dundee

Mechanical Evidence of the Orbital Angular Momentum to Energy Ratio of Vortex Beams

Demore, Christine E. M.; Yang, Zhengyi; Volovick, Alexander; Cochran, Sandy; MacDonald, Michael P.; Spalding, Gabriel C.

Document Version
Publisher's PDF, also known as Version of record

Link to publication in Discovery Research Portal

Mechanical Evidence of the Orbital Angular Momentum to Energy Ratio of Vortex Beams

Christine E. M. Demore,[1] Zhengyi Yang,[1] Alexander Volovick,[1,2] Sandy Cochran,[1]
Michael P. MacDonald,[1] and Gabriel C. Spalding[3]

[1]*Institute for Medical Science and Technology, University of Dundee, DD2 1FD Dundee, United Kingdom*
[2]*InSightec Ltd., Tirat Carmel 39120, Israel*
[3]*Department of Physics, Illinois Wesleyan University, Bloomington, Illinois 61701, USA*

We measure, in a single experiment, both the radiation pressure and the torque due to a wide variety of propagating acoustic vortex beams. The results validate, for the first time directly, the theoretically predicted ratio of the orbital angular momentum to linear momentum in a propagating beam. We experimentally determine this ratio using simultaneous measurements of both the levitation force and the torque on an acoustic absorber exerted by a broad range of helical ultrasonic beams produced by a 1000-element matrix transducer array. In general, beams with helical phase fronts have been shown to contain orbital angular momentum as the result of the azimuthal component of the Poynting vector around the propagation axis. Theory predicts that for both optical and acoustic helical beams the ratio of the angular momentum current of the beam to the power should be given by the ratio of the beam's topological charge to its angular frequency. This direct experimental observation that the ratio of the torque to power does convincingly match the expected value (given by the topological charge to angular frequency ratio of the beam) is a fundamental result.

Angular momentum in vortex beams.—That light carries momentum is well known from the work of both Planck and Einstein and since the 1970s this principle has been regularly observed in the lab in optical manipulation experiments [1–3]. Light has also been shown to carry angular momentum: spin angular momentum related to the polarization state of the light and, more recently, orbital angular momentum, as a result of helicity in the phase fronts of the light [4–8]. The orbital angular momentum, L_z, of a single photon is simply $l\hbar$, such that the quantity of orbital angular momentum carried by a beam is linearly proportional to the topological charge, l. Transfer of this orbital angular momentum has been observed in "optical spanner" experiments in which a focused Laguerre-Gaussian beam is absorbed by a microscopic particle, leading the particle to rotate at a rate proportional to the beam's topological charge [9]. Although this dependence can be observed mechanically for a continuous flux of photons in a focused laser beam, L_z has only ever been measured indirectly for a single photon [10].

Closely linked to the angular momentum of a photon is its energy, $E = \hbar\omega$. Hence the ratio L_z/E of a single photon is simply l/ω. This ratio holds for phonons as well because the angular momentum of a phonon is also $l\hbar$ with an energy $\hbar\omega$. However, unlike photons, phonons cannot carry spin angular momentum in fluids because they have no polarization. The transfer of orbital angular momentum from acoustic fields has been shown in two parallel studies [11–13], but both studies used coarsely discretized sources. In the present study, we use a 1000-element matrix array transducer to produce a range of fully

propagating beams of different topological charge in order to test the dependence of L_z upon l and the total energy in the beam.

When observing the transfer of angular momentum, the key characteristic of the beam is in fact the time average of the angular momentum current, $\langle \dot{L}_z \rangle$ because the transfer of the extremely small amounts of momentum carried by a single phonon or photon is prohibitively difficult to observe. When a vortex beam impinges upon an object, some or all of $\langle \dot{L}_z \rangle$ is absorbed, leading to a rate of change of angular momentum dL_z/dt. dL_z/dt is also the definition for the torque, Γ, exerted upon an object. It has been predicted [13–16] that

$$\frac{\langle \dot{L_Z} \rangle}{P} = \frac{l}{\omega_B}, \tag{1}$$

where P is the total power in the beam and ω_B is the angular frequency of the beam. P can be measured from the levitation force exerted upon an object in a fluid-filled chamber open to the atmosphere, multiplied by the speed of sound in the fluid (1482 m/s for water at room temperature), such a force balance being the standard method to accurately measure the power in a beam [17,18]. Hence, by measuring the ratio of the torque exerted by a beam on an object to its levitation force, we can directly measure the ratio of orbital angular momentum to energy of a helical beam.

Though this ratio is a fundamental basis for much of physics and is essentially taken for granted, it has never previously been directly observed in a single experiment. In the case of optics this is largely because it is difficult to

be sure of the relative efficiencies of the transfer of linear and angular momentum, as one is a result of scattering (high efficiency) and the other absorption (lower efficiency). Added to this is the fact that the beam has to be focused very tightly for optical trapping, introducing a wide range of incident angles and a significant subsequent perturbation to the helical wave fronts. In acoustics, this has also not been seen before, as existing studies used only low order ($\pm l = 1, 2$) helical acoustic fields and were not able to produce a range of propagating "Laguerre-Gaussian" (LG) acoustic beams of varying l. In this study we use a matrix array to produce a range of fully characterized acoustic vortex beams with variable topological charges, l, and focusing regimes [19]. These beams are used to both levitate and rotate an acoustic absorber such that P can be measured from the levitation force and $\langle \dot{L}_z \rangle$ from the torque exerted upon the absorber. Since the transfer of momentum is a result of absorption for both angular and linear momentum, and highly acoustically absorbent materials are available, we are able to use these measurements to calculate the ratio of $\langle \dot{L}_z \rangle$ to P.

Experiment.—The setup for measuring the rotation and levitation of a target in an acoustic vortex is shown in Fig. 1. A high intensity focused ultrasound (HIFU) array system (ExAblate 2100, InSightec, Israel) is used to produce the beam. The matrix array is placed underneath an optically transparent chamber with an acoustically transparent Mylar base. The chamber is filled with degassed water to avoid cavitation during the experiments and the transducer placed in a separate chamber, coupled to the first chamber by a thin layer of water. The target, a 100 mm diameter, 10 mm thick disk of acoustic absorber material (Aptflex F28, Precision Acoustics, Dorchester, UK) with a mass of 87 g, is attached to a 5 ml syringe to allow stable rotation and levitation about a rod attached to the optically transparent lid of the chamber. The rod serves only to stabilize the rotation, and does not exert any vertical forces on the target (except for friction, which does not affect its
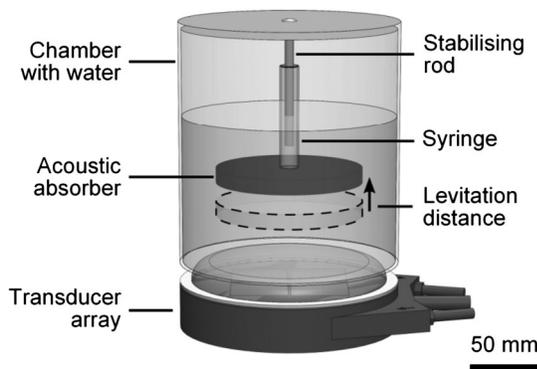

FIG. 1.   Diagram of experimental setup for levitating and rotating acoustic absorber target using 550 kHz ultrasonic matrix transducer array at the base of a chamber filled with degassed water.

equilibrium position). With no acoustic field applied, the absorber or syringe assembly reaches a neutrally buoyant position approximately 35 mm above the array. Video cameras are positioned above and at one side of the chamber to capture the rotation and levitation of the acoustic absorber target, respectively.

The array consists of a 550 kHz matrix array system, with approximately 1000 elements in a 74 mm square aperture, and has been designed to enable focusing and steering of a high power continuous wave (CW) beam within a large volume of interest. The array elements are individually addressable, with the phase discretized to increments of $\pi/4$ by the control software. In the experiments presented here, the phase, active aperture, and transmitted acoustic power are specified directly, in close analogy with the use of a spatial light modulator (SLM) to produce an LG beam in optics.

Examples of phase profiles applied to the array elements are shown in Fig. 2 (column 1). A circular subaperture of the matrix array was used to produce cylindrically shaped beams. For an unfocused beam, only periodic azimuthal phases are applied, as shown in Fig. 2(a), and the absorber is in the near field of the array. For focused beams, radial phase profiles for focusing at a specified distance are added to the azimuthal phases before phase discretization. The addition of the focusing phases causes the spiral pattern shown in Figs. 2(f), 2(k), and 2(p).

The angular spectrum method [20] can be used to calculate the ultrasound field in planes transverse to the propagation direction, given the phase and amplitude profile of the transmitting array. Complex pressure profiles predicted with this method at 60 mm from the array are shown in Fig. 2 (columns 2, 3) for the example source phase profiles in Fig. 2 (column 1). Complex pressure profiles measured with a hydrophone, shown in Fig. 2 (columns 4, 5), are qualitatively very similar to the predicted profiles. The predicted and measured normalized pressure amplitude profiles show clearly the axial null at the phase singularity. Because of the source geometry, the form of the pressure maximum region is not an ideal annulus, but localized to four corners. The calculated pressure profiles show that this squaring effect reduces, and the diameter of the annulus increases, with higher order beams. Focusing reduces the diameter and the width of the pressure density annulus. Figures 2(p)–2(r) demonstrate that despite the finite number of source elements, high order ($l = -12$) helical beams can be produced without evidence of aliasing.

When beams such as those shown in Fig. 2 impinge upon the absorber they are almost entirely absorbed ($> 95\%$) and the absorber is seen to levitate to a new equilibrium position and rotate for the duration of the sonication (see videos in supplementary material at [21]). The acoustic radiation force on the target because of an incident acoustic beam is determined from the apparent change in
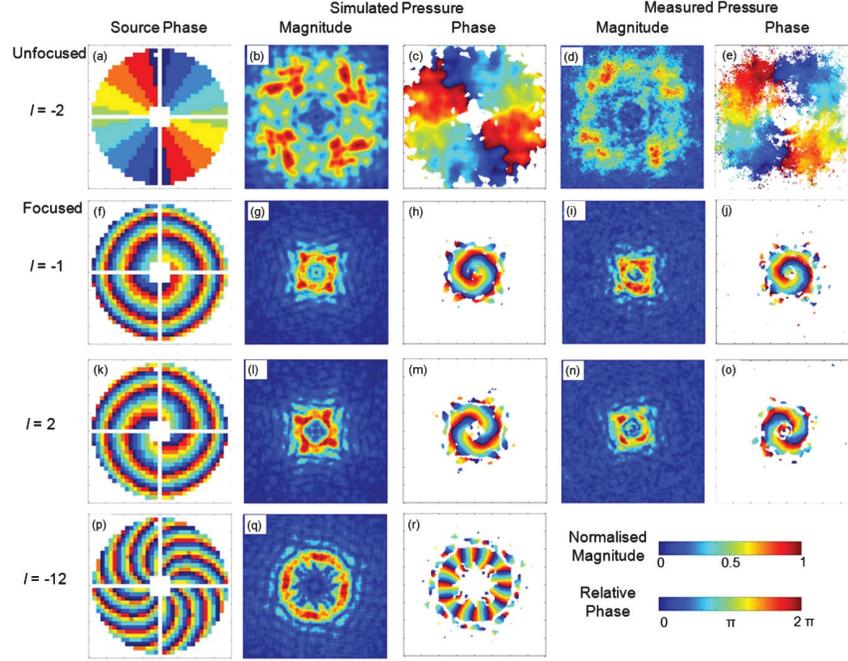
FIG. 2 (color).   Applied phase profile of transducer array, and simulated and measured pressure of helical beams with topological charge l at a plane approximately 60 mm above the transducer face. [(a)–(e)] $l = -2$, unfocused beam. (f)–(j) $l = -1$, focused at 100 mm. [(k)–(o)] $l = 2$, focused at 100 mm. [(p)–(r)] $l = -12$, focused at 100 mm. Displayed region is 80 mm square. Pressure amplitude threshold used in phase maps is 0.25 of peak amplitude.

the buoyancy force. The axial force, F_z, from the acoustic beam is given by

$$F_z = \rho g A d, \qquad (2)$$

where ρ is the density of water (1000 kg m^{-3}), g is the acceleration due to gravity, and A is the cross-sectional area of the syringe, which relates to the column of displaced water. The target levitation distance, d, the height difference between its position at rest and at equilibrium during sonication, was measured from the side-view videos using the graduated marks on the syringe. The measured acoustic radiation force is shown in Fig. 3(a). It increases with transmitted acoustic power, decreases with topological charge, and does not vary significantly with focal distance.

A decrease in radiation force with l is expected from simulation of the incident beam power. The measured acoustic radiation force decreases between 20% and 40% over the range of topological charge because the limited number of transducer elements makes it increasingly difficult for the array to produce a smooth phase profile for higher order beams, and any phase aberration will reduce the levitation force [22]. Any perturbation of the phase profile at a given location in the beam affects both the axial and azimuthal components of the net Poynting vector, and yet the ratio of the angular momentum current to total power can still be measured [23].

The top view camera allowed us to observe the rotational motion from the acceleration phase through to terminal angular velocity. The differential equation for this rotational motion is given by

$$\Gamma_B = I\ddot{\theta} - C\dot{\theta}, \qquad (3)$$

where Γ_B is the torque applied by the beam, equal to the angular momentum current from the beam into the absorber, $\langle \dot{L}_z \rangle$, I is the moment of inertia of the absorber about its axis of rotation, θ is the angular displacement, and C is the drag coefficient. Drag is assumed to be linear as angular velocities are low. This equation of motion is the same as that for a vertical fall through a fluid and as a result has a similar solution:

$$\theta = \theta_0 + \omega_A(t - t_0) + [1 - e^{-(t-t_0)/\tau}] + \omega_A[e^{-(t-t_0)/\tau} - 1], \qquad (4)$$

where θ_0 is the initial angular position, ω_A is the terminal angular velocity, ω_0 is the initial velocity, t_0 is the time at which sonication begins and $\tau = I/C$ is the characteristic time of the acceleration phase. Once the terminal velocity is reached, such that $t \gg \tau$ the applied torque is balanced by the drag torque and, Eq. (4) reduces to a linear function with an intercept θ_0 and slope ω_A. Using only data taken at equilibrium, ω_A and subsequently the angular momentum of the absorber, as seen in Fig. 3(b), can be obtained for all data sets. The transferred angular momentum increases with transmitted acoustic power, and, while it increases with l, the relationship is not linear because of the lower incident beam power at higher topological charges.
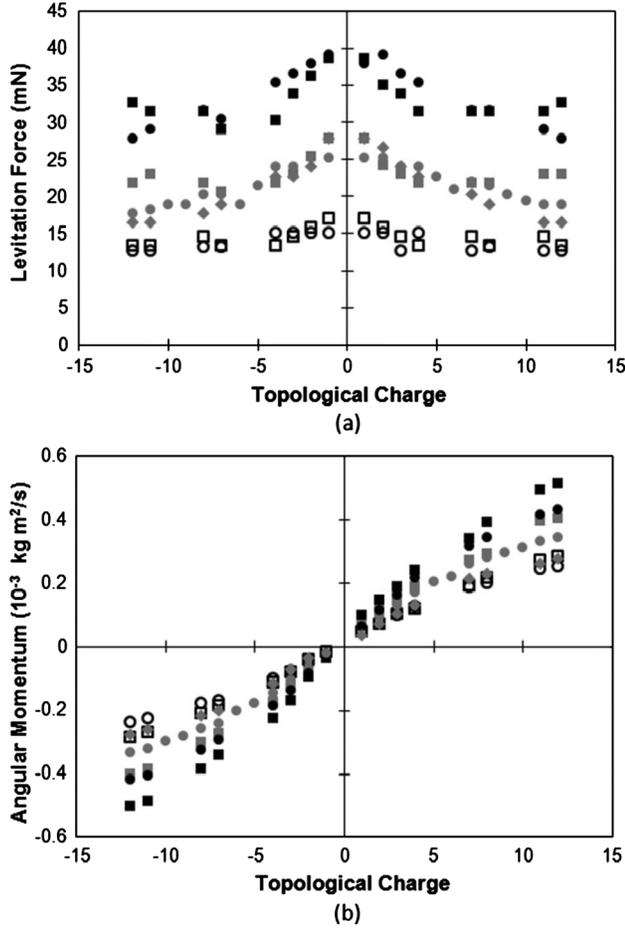
FIG. 3. (a) Ultrasonic levitation force on and (b) angular momentum transferred to acoustic absorber from helical ultrasonic beams focused at $f = 70$ (◆), 100 mm (●), or unfocused (■), and transmitted acoustic power of 23 W (outline), 39 W (gray), or 55 W (black), and topological charge $l = \pm1 - 12$.
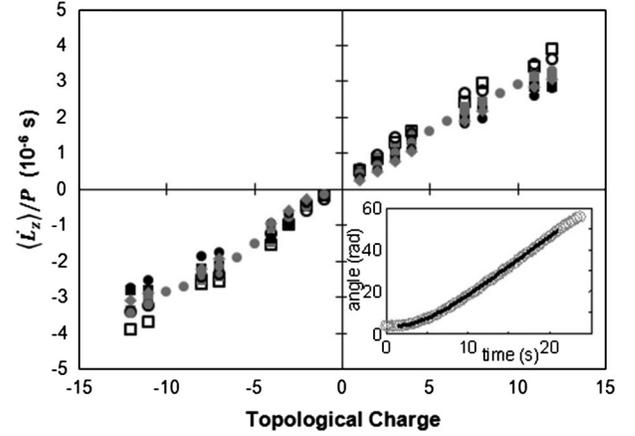

FIG. 4. Ratio of measured torque to power incident on acoustic absorber from a range of helical ultrasonic beams focused at $f = 70$ (◆), 100 mm (●), or unfocused (■), and transmitted acoustic power of 23 W (outline), 39 W (gray), or 55 W (black), and topological charge $l = \pm1 - 12$. The inset shows an example of the equation of motion fit to the angular position of the absorber.

calculate the drag coefficient of the absorber purely from terminal angular velocity.

In conclusion, within the error margin of the experiment, we have confirmed, using simultaneous measurements, that the predicted torque to power ratio holds. Therefore, the relationship of linear to orbital angular momentum in a helical beam is as predicted by theory.

The drag coefficient used to calculate $\langle \dot{L}_z \rangle$ is determined by fitting the complete form of Eq. (4) to full data sets in which the acceleration phase is unperturbed. An example data set for the absorber motion and the fit to Eq. (4), using ω_A determined from the linear fit at equilibrium, is shown in the inset of Fig. 4; the close fit to the data confirms that the assumption of linear drag is valid. This yields an average value for C of $(2.9 \pm 0.2) \times 10^{-5}$ kg m^{2}s^{-1}.

The ratio of $\langle \dot{L}_z \rangle / P$ is shown in Fig. 4, and as predicted by theory, all data sets lie on a straight line. The slope of the linear fit [which according to Eq. (1) should be $1/\omega_B$] to all the data in Fig. 4 is $(2.87 \pm 0.05) \times 10^{-7}$ s. For the 550 kHz array, the $1/\omega_B$ slope should be 2.89×10^{-7}, confirming the validity of the predicted ratio of orbital angular momentum to energy. As further verification of this, if we assume the ratio in Eq. (1) to be valid and rearrange, we can obtain C from the inverse of the slope of the linear fit to all the data, yielding a value of $(2.97 \pm 0.02) \times 10^{-5}$ kg m^2 s^{-1}. Hence, it is also possible to

[1] A. Ashkin, Phys. Rev. Lett. **24**, 156 (1970).
[2] D. G. Grier, Nature (London) **424**, 810 (2003).
[3] K. Dholakia and T. Čižmár, Nature Photon. **5**, 335 (2011).
[4] L. Allen, M. W. Beijersbergen, R. J. C. Spreeuw, and J. P. Woerdman, Phys. Rev. A **45**, 8185 (1992).
[5] H. He, M. E. J. Friese, N. R. Heckenberg, and H. Rubinsztein-Dunlop, Phys. Rev. Lett. **75**, 826 (1995).
[6] M. E. J. Friese, T. A. Nieminen, N. R. Heckenberg, and H. Rubinsztein-Dunlop, Nature (London) **394**, 348 (1998).
[7] J. F. Nye and M. V. Berry, Proc. R. Soc. A **336**, 165 (1974).
[8] M. P. MacDonald, P. Prentice, and K. Dholakia, New J. Phys. **8**, 257 (2006).
[9] N. B. Simpson, K. Dholakia, L. Allen, and M. J. Padgett, Opt. Lett. **22**, 52 (1997).

[10] J. Leach, M. J. Padgett, S. M. Barnett, S. Franke-Arnold, and J. Courtial, Phys. Rev. Lett. **88,** 257901 (2002).

[11] K. Volke-Sepúlveda, A. O. Santillán, and R. R. Boullosa, Phys. Rev. Lett. **100,** 024302 (2008).

[12] A. O. Santillán and K. Volke-Sepúlveda, Am. J. Phys. **77,** 209 (2009).

[13] K. D. Skeldon, C. Wilson, M. Edgar, and M. J. Padgett, New J. Phys. **10,** 013018 (2008).

[14] B. T. Hefner and P. L. Marston, J. Acoust. Soc. Am. **106,** 3313 (1999).

[15] J. Lekner, J. Acoust. Soc. Am. **120,** 3475 (2006).

[16] L. K. Zhang and P. L. Marston, Phys. Rev. E **84,** 065601 (R) (2011).

[17] T. Hasegawa and K. Yosioka, J. Acoust. Soc. Am. **58,** 581 (1975).

[18] R. T. Beyer, J. Acoust. Soc. Am. **63,** 1025 (1978).

[19] G. C. Spalding, A. Volovick, Z. Yang, C. Demore, M. P. MacDonald, and S. Cochran, in *Proceedings of Optical Trapping and Optical Micromanipulation VIII,* edited by K. Dholakia and G. C. Spalding (SPIE, Bellingham, WA, 2011), p. 80971N.

[20] E. G. Williams, *Fourier Acoustics: Sound Radiation and Nearfield Acoustical Holography* (Academic Press, London, 1999), p. 31.

[21] See Supplemental Material at http://link.aps.org/supplemental/10.1103/PhysRevLett.108.194301 for details.

[22] Y. Hertzberg, A. Volovick, Y. Zur, Y. Medan, S. Vitek, and G. Navon, Med. Phys. **37,** 2934 (2010).

[23] J. Leach, S. Keen, M. J. Padgett, C. Saunter, and G. D. Love, Opt. Express **14,** 11919 (2006).